

Glass transition and crystallization kinetics of a barium borosilicate glass by a non-isothermal method

Andreia A. S. Lopes, Roque S. Soares, Maria M. A. Lima, and Regina C. C. Monteiro

Citation: *Journal of Applied Physics* **115**, 043516 (2014); doi: 10.1063/1.4863334

View online: <http://dx.doi.org/10.1063/1.4863334>

View Table of Contents: <http://scitation.aip.org/content/aip/journal/jap/115/4?ver=pdfcov>

Published by the [AIP Publishing](#)

Articles you may be interested in

[Low-temperature properties of monoalcohol glasses and crystals](#)

Low Temp. Phys. **39**, 468 (2013); 10.1063/1.4807147

[Kinetics of amorphous-crystallization transformation of Se 85 x Te 15 Sn x \(x = 2, 4 and 6\) alloys under non-isothermal conditions using Matusita's approach](#)

AIP Conf. Proc. **1512**, 542 (2013); 10.1063/1.4791151

[Crystallization of amorphous Cu 47 Ti 34 Zr 11 Ni 8](#)

J. Appl. Phys. **89**, 1573 (2001); 10.1063/1.1332089

[Crystallization kinetics and structural aspects of TeGaSn amorphous alloys](#)

J. Appl. Phys. **88**, 3276 (2000); 10.1063/1.1288691

[Differential scanning calorimetry, x-ray diffraction and ¹⁹F nuclear magnetic resonance investigations of the crystallization of InF 3 -based glasses](#)

J. Chem. Phys. **109**, 2432 (1998); 10.1063/1.476812



Re-register for Table of Content Alerts

Create a profile.



Sign up today!



Glass transition and crystallization kinetics of a barium borosilicate glass by a non-isothermal method

Andreia A. S. Lopes, Roque S. Soares, Maria M. A. Lima, and Regina C. C. Monteiro^{a)}

Department of Materials Science, CENIMAT/I3N, Faculty of Sciences and Technology, Universidade Nova de Lisboa, 2829-516 Caparica, Portugal

(Received 17 November 2013; accepted 13 January 2014; published online 28 January 2014)

The glass transition and crystallization kinetics of a glass with a molar composition $60\text{BaO}-30\text{B}_2\text{O}_3-10\text{SiO}_2$ were investigated by differential scanning calorimetry (DSC) under non-isothermal conditions. DSC curves exhibited an endothermic peak associated with the glass transition and two partially overlapped exothermic peaks associated with the crystallization of the glass. The dependence of the glass transition temperature (T_g) and of the maximum crystallization temperature (T_p) on the heating rate was used to determine the activation energy associated with the glass transition (E_g), the activation energy for crystallization (E_c), and the Avrami exponent (n). X-ray diffraction (XRD) revealed that barium borate ($\beta\text{-BaB}_2\text{O}_4$) was the first crystalline phase to be formed followed by the formation of barium silicate ($\text{Ba}_5\text{Si}_8\text{O}_{21}$). The variations of activation energy for crystallization and of Avrami exponent with the fraction of crystallization (χ) were also examined. When the crystallization fraction (χ) increased from 0.1 to 0.9, the value of local activation energy ($E_c(\chi)$) decreased from 554 to 458 kJ/mol for the first exothermic peak and from 1104 to 831 kJ/mol for the second exothermic peak. The value determined for the Avrami exponent was near 2 indicating a similar one-dimensional crystallization mechanism for both crystalline phases. This was confirmed by the morphological studies performed by scanning electron microscopy (SEM) on glass samples heat-treated at the first and at the second crystallization temperatures. © 2014 AIP Publishing LLC. [<http://dx.doi.org/10.1063/1.4863334>]

I. INTRODUCTION

Borosilicate glasses, due to their chemical stability, low softening temperature, low dielectric constant, and high electrical resistance, are of great interest for diversified technological applications in electronic industries, such as display panels, low-temperature co-fired ceramics, and packaging.¹⁻⁶ At present, the selection of borosilicate glasses with low sintering temperature has been expanding to meet stringent requirements and to reduce manufacturing costs. In order to obtain glasses with low sintering temperatures, some alkali or bivalent metal oxides must be added.^{2,3,7,8}

PbO containing glass systems, due to their low glass transition temperature, high structural stability, and good electrical and thermal characteristics, were considered as high efficiency candidates for low sintering temperature processes. However, due to several environmental concerns, recent regulations have restricted the use of PbO.^{2,9} BaO has been employed as a candidate material for PbO replacement, particularly in the ternary system $\text{PbO}-\text{B}_2\text{O}_3-\text{SiO}_2$.^{2-5,9} In a recent work of some of the authors, lead-free borosilicate glasses based on the quaternary $\text{BaO}-\text{ZnO}-\text{B}_2\text{O}_3-\text{SiO}_2$ system have been investigated regarding their sintering and crystallization behaviour.⁸ PbO containing glasses do not crystallize easily, but the addition of other glass modifiers can result in the crystallization of the glasses during the sintering process.^{2,8,10} Therefore, in order to optimize the processing parameters, it is important to understand the crystallization kinetics and mechanisms of nucleation and growth.

Although in recent years there has been a significant effort in developing barium borosilicate based glasses and glass-ceramics for a wide range of technological applications,^{1,2,10-13} a reduced amount of work has been devoted to investigate the crystallization kinetics of such glasses and almost exclusively to study sealant glassy materials that contain extra modifier oxides (e.g., ZnO, MgO, CaO).^{11,12,14-16} The structure of barium borosilicate glasses has been investigated by some authors using different techniques such as magic angle spinning nuclear magnetic resonance (MAS NMR), Raman and Fourier-transform infrared (FTIR) spectroscopy.^{1,13,17-20} These studies have shown the existence of structural units like trigonally coordinated boron (BO_3), tetrahedrally coordinated boron (BO_4), and silicon structural units having different number of bridging oxygen atoms.^{1,13,17} The addition of BaO to borosilicate glasses results in the conversion of BO_3 to BO_4 structural units,^{1,13,17} and the fraction of non-bridging oxygen atoms increases with the amount of BaO.^{1,13,17,18} The increase in the fraction of non-bridging oxygen atoms leads to a more opened structure and consequently lowers the glass transition temperature.^{1,2} The decrease in the glass crystallization temperature is also believed to be caused by the breakdown of the glass network structures.^{1,2}

Studies of the glass transition and of crystallization kinetics in amorphous materials can be interpreted in terms of several proposed theoretical models and equations. Differential scanning calorimetry (DSC) is a very useful tool to investigate the glass transition and the crystallization kinetics of glassy materials, allowing the possibility of obtaining data with isothermal and non-isothermal methods.^{11,12,14-16,21-24} From the dependence of the glass

^{a)}Electronic mail: rcm@fct.unl.pt

transition temperature (T_g) on the heating rate, the activation energy associated with the glass transition (E_g) has been calculated.^{25,26} From the dependence of the peak temperature for crystallization (T_p) on the heating rate, the most important kinetic parameters for crystallization have been calculated, the activation energy for crystallization (E_c) and the Avrami exponent (n) that depends on the mechanism and dimensionality of the crystal growth.^{11,12,14–16,21–24}

The activation energy associated with the glass transition can be determined using Kissinger²⁵ and Moynihan²⁶ methods. The crystallization kinetics can be investigated using the formal theory of transformation kinetics proposed by Johnson and Mehl²⁷ and Avrami,^{28–30} (JMA model) that is valid only under isothermal conditions. The non-isothermal method is more simple and quicker than the isothermal method.^{21,22,24} Experimental results obtained from non-isothermal thermoanalytical studies have been used to determine the crystallization parameters according to different methods.³¹ To interpret the non-isothermal data, the approaches developed by the various models assume that the variation of the peak crystallization temperature is directly related to the heating rate employed in the experiment.^{31–35}

In view of the above-mentioned perspective, the glass transition and crystallization kinetics of a barium borosilicate glass with a molar composition 60BaO-30B₂O₃-10SiO₂ were investigated by DSC under non-isothermal conditions using different methods. This ternary glass composition was investigated regarding its potential interest for application as a Pb-free low temperature sinterable glass and because, according to previous work,⁸ it crystallizes easily during sintering. The crystalline phases were identified by X-ray diffraction (XRD) and the microstructure of the crystallized glasses was investigated by scanning electron microscopy (SEM). The nucleation and growth of crystalline phases in the glass matrix is described and analysed.

II. EXPERIMENTAL PROCEDURE

The 60BaO-30B₂O₃-10SiO₂ glass was prepared by the conventional melt-quenching route. The starting materials were BaCO₃ (BDH), H₃BO₃ (Merck), and SiO₂ (BDH) powders, all of them with a purity higher than 99%. The proper amount of each material was weighed and mixed for 30 min in a teflon jar, using a laboratory powder mixer (turbula WAB, T2F). Then, the mixture was melted in platinum crucible in an electric furnace at 1723 K for 2 h in air. Finally, the molten glass was quenched into cold distilled water to avoid crystallization and to form a glass frit.

Glass powders were obtained by milling the glass frit (~20 g) with absolute ethanol for 2 h using an agate ball mill (Fritsch, Pulverizette), with a 80 ml capacity container and 3 balls of ϕ 20 mm and 5 balls of ϕ 10 mm, weight ratio of sample/balls=0.5, rotating at constant speed of 600 rpm. After drying, the powder by was sieved to obtain a glass powder fraction with a particle size smaller than 65 μ m that was used in all experiments.

The DSC tests were carried out using 50 mg glass powder samples heated in alumina crucible in static air (Linseis STA PT1600) from room temperature to 700 K at different

heating rates ($\beta = 5, 10, 15,$ and 20 K/min). Measured DSC data were corrected by subtracting a blank measurement made without sample under the same conditions, and automatic baseline correction was performed with the software package delivered with the thermal analysis equipment. The glass transition temperature (T_g), the onset temperature of crystallization (T_c), and the peak crystallization temperature (T_p) for the investigated glass were determined from the DSC data by using the microprocessor of the thermal analyzer, the measurement error being assumed as 1%.

The glass powders were uniaxial pressed using a compressive stress of ~75 MPa and the resulting compacts (~3 mm height, 13 mm diameter) were heat treated in an electric tubular furnace from room temperature up to a selected temperature suggested by the DSC results. The samples were held during 60 min at that temperature and then were left to cool inside the furnace.

The amorphous nature of the glass powder and the crystalline phases present in heat-treated glass samples were identified by XRD analysis (DMAX-IIIC diffractometer-Rigaku Industrial Corporation), using CuK α radiation (40 kV, 30 mA), 2θ angle range 10°–60°, a scanning rate of 2° min⁻¹ and a sampling interval of 0.01° (2θ). The phases were identified by comparing the experimental X-ray patterns to standards complied by the International Centre for Diffraction Data (ICDD).

Microstructural observations of the sintered glass samples were performed by SEM (ZEISS, DSM 960). SEM observations were carried out in polished surfaces (mirror finishing) and some of them were etched by immersion in 2 vol. % HF solution for 2 s. Au/Pd surface coating was used to avoid electric charging.

III. RESULTS AND DISCUSSION

A. Structural and thermal studies

Melting at 1723 K for 2 h was adequate to obtain glass as the XRD pattern of the as-quenched glass (Figure 1)

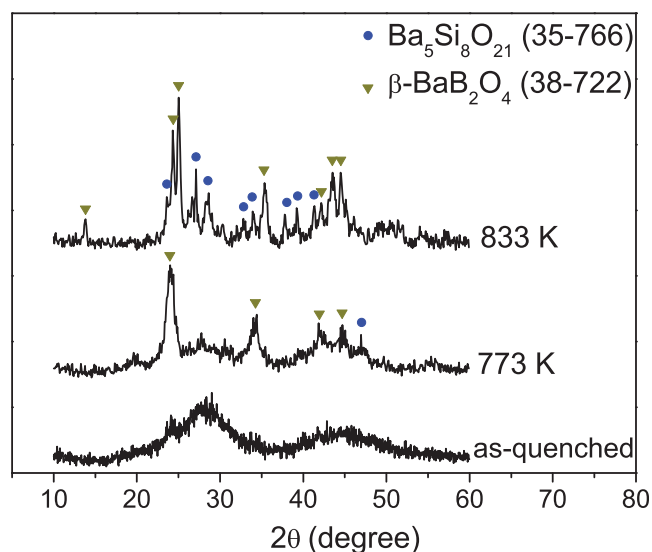


FIG. 1. XRD patterns for the as-quenched glass and for heat-treated glass samples.

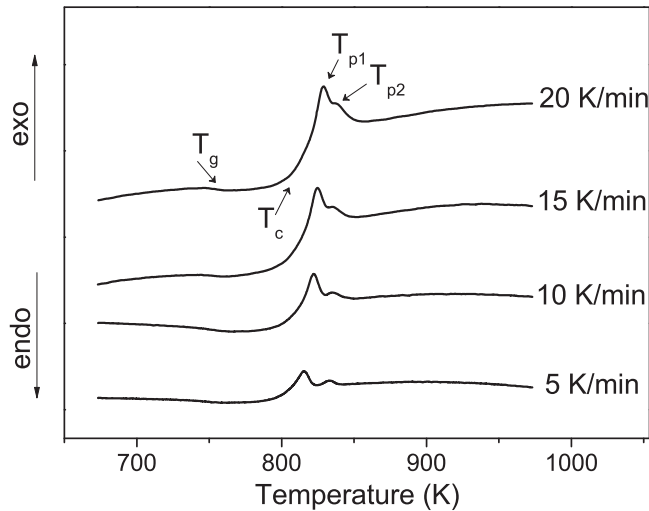


FIG. 2. DSC curves for the glass powder obtained at different heating rates.

confirmed its amorphous nature. Two broad peaks are clearly observed, approximately at $2\theta = 28^\circ$ and 43° , which is the characteristic of borate glasses containing a high level of BaO plus B_2O_3 (totalizing ≈ 90 mol. %) ^{1,2,8}. The as-quenched glass appeared slightly opalescent and this is likely due to phase separation as it appeared that two distinct amorphous structures coexisted as revealed by the double hump in the XRD pattern. According to some structural models of alkali borosilicate glasses reported in literature, ³⁶ the glass is composed of two micro-phase separated borate and silicate networks, in which the sharing of the modifier between the two networks depends on the relative amounts of borate structural units. ^{20,36}

Figure 2 shows the DSC curves for the glass powder obtained at various heating rates. The change with the heating rate of T_g (corresponding to a shift on the base line), of T_c and of T_{p1} and T_{p2} (these ones corresponding to the first and second exothermic peaks observed in every curve) is presented in Table I.

It is observed that the characteristic temperatures of the glass (T_g , T_c , and T_p) increase with the increase in the heating rate and that the thermal stability, (temperature gap $\Delta T = T_c - T_g$), which corresponds to the interval in which structural rearrangements are allowed without the occurrence of crystallization, decreases from 78 to 55 K when the heating rate increases from 5 to 20 K/min. The difference between T_{p1} and T_g is low (79–95 K), meaning that it is a rapid crystallizing glass. ^{15,17}

Figure 3 shows a magnification of the crystallization exotherms for the DSC curve obtained at a heating rate (β)

TABLE I. Glass transition (T_g), onset crystallization (T_c), and maximum crystallization (T_{p1} and T_{p2}) temperatures determined from DSC data obtained at different heating rates (β).

β (K/min)	T_g (K)	T_c (K)	T_{p1} (K)	T_{p2} (K)
5	720	798	815	833
10	734	802	822	835
15	745	803	825	837
20	750	805	829	838

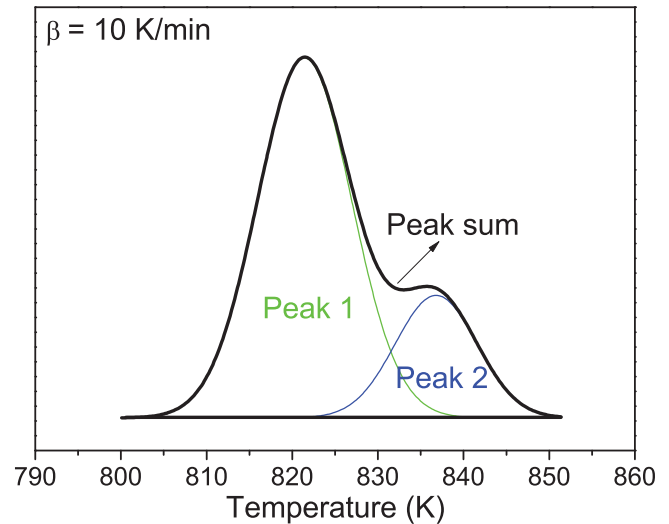


FIG. 3. Separation of overlapped crystallization peaks in the crystallization exotherm obtained at $\beta = 10$ K/min.

of 10 K/min and the separation of the two overlapping crystallization peaks is illustrated. The software used for exotherm peak fitting was OriginPro 8. Modeling of the experimental DSC curve was carried out using two partially overlapping Gaussian curves.

The XRD patterns of glass samples heat treated at two different temperatures are also shown in Figure 1. With the increase in the heat treatment temperature, a higher intensity of the diffraction peaks and a better development of the crystals are revealed. XRD results shown in Figure 1 indicate that, in a glass samples heat-treated at $T = 773$ K ($T_c < T < T_{p1}$, for $\beta = 5$ K/min), the diffraction peaks correspond to a crystalline phase identified as barium borate (β -BaB₂O₄, JCPDS File 38-0722), while in samples heated at $T = 833$ K ($T_{p1} < T < T_{p2}$, for $\beta = 5$ K/min) an additional crystalline phase is also identified, barium silicate (Ba₅Si₈O₂₁, JCPDS File 35-0766). These results indicate that the formation of the two crystalline phases can be ascribed to the two overlapping crystallization peaks in the DSC curves. The formation of these two crystalline phases, barium borate (β -BaB₂O₄) and barium silicate (Ba₅Si₈O₂₁) can be correlated with the structural features of the 60BaO-30B₂O₃-10SiO₂ glass, consisting of various main constructional units, borate structural units and silicate structural units. According to literature, ^{1,13,18} structural analysis carried out for barium borosilicate glasses showed that increasing of BaO content results in the conversion of boroxyl groups (BO₃) into groups containing BO₄ units and that the silicate glass network becomes more depolymerized with the increase on the concentration of non-bridging oxygen atoms.

B. Glass transition analysis

The dependence of the glass transition temperature (T_g) on the heating rate (β) can be approached by several equations. In previous works, ^{37,38} where glasses based on different composition were investigated, it has been described using the empirical relationship suggested by Lasocka, ³⁷ which is expressed as

$$T_g = A_g + B_g \log \beta, \quad (1)$$

where A_g and B_g are constants for a given glass composition. The value for A_g represents the glass transition temperature at a heating rate of 1 K/min. The value for the constant B_g has been related to the method of quenching the glass,³⁷ the lower the cooling rate of the melt, the lower the B_g value.³⁷⁻⁴⁰ The plot of T_g versus $\log(\beta)$ and a straight regression line fitted to the DSC experimental data are shown in Figure 4. The inset in Figure 4 shows an upward shift in T_g with increasing heating rate, and the change of T_g with β is also presented in Table I. For the current glass, the values determined for A_g and B_g are 684.3 K and 50.8 K, respectively, and so the empirical formula can be written in the form

$$T_g = 684.3 + 50.8 \log \beta. \quad (2)$$

A second approach regarding the dependence of the glass transition temperature on the heating rate is based on Kissinger's method,²⁵ which considers the following relationship:

$$\ln\left(\frac{T_g^2}{\beta}\right) = \frac{E_g}{RT_g} + \text{constant}, \quad (3)$$

where R is the universal gas constant and E_g is the activation energy associated with the glass transition.⁴⁰ Although XRD results for the as-quenched glass indicated two distinct amorphous structures, only a single T_g was identified in the DTA curves (see Figure 1 and inset in Figure 4) and therefore it was considered appropriate to apply Eq. (3) for the determination of E_g . Despite the fact that such expression has been originally deduced for the crystallization kinetics, it has often been used to calculate the activation energy for the glass transition that involves the molecular motion and rearrangement of atoms around the glass transition temperature.³⁹ According to Eq. (3), a plot of $\ln(T_g^2/\beta)$ versus $1/T_g$ should be a straight line, and from its slope the value of E_g can be determined. A plot of $\ln(T_g^2/\beta)$ versus $1000/T_g$ for the

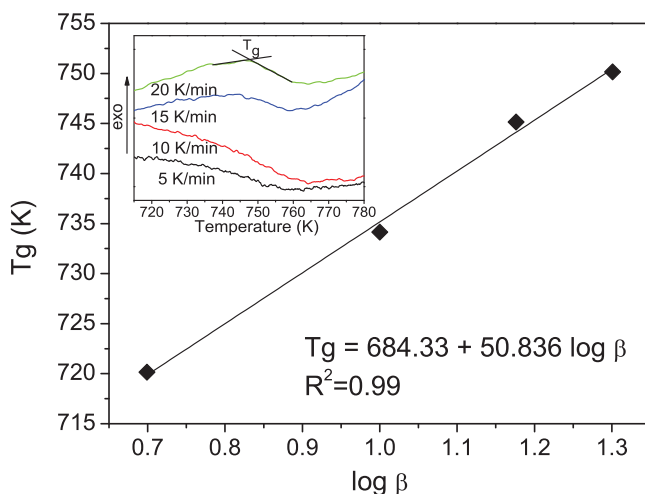


FIG. 4. T_g versus $\log \beta$ for the as-quenched glass. The inset depicts the glass transition peaks observed at various heating rates.

studied glass is shown in Figure 5, displaying the linearity of the used equation. From the slope of the straight line, the value of E_g was calculated, and it is equal to 190 kJ/mol.

Another approach to determine the value of E_g is based on a simplified form of Eq. (3), since it has been assumed that the variation of $\ln(1/T_p^2)$ with $\ln \beta$ is much slower than that of $\ln(1/T_p)$ with $\ln \beta$, resulting in the following relationship:^{26,41}

$$-\ln(\beta) = \frac{E_g}{RT_g} + \text{constant}. \quad (4)$$

The plot of $\ln(\beta)$ versus $1/T_g$ is also presented in Figure 5. In this case, the value obtained for E_g is equal to 202 kJ/mol, which is in good agreement with that obtained by the Kissinger equation. From the above two values, the activation energy of glass transition is around 196 kJ/mol.

C. Crystallization kinetics

The crystallization process was evaluated using different non-isothermal methods, employing the DSC results obtained at different heating rates, and the kinetic parameters (activation energy for crystallization, E_c , and Avrami exponent, n) for the first and the second crystallization peaks were determined. Kissinger method,²⁵ beyond its use in the determination of the activation energy for glass transition, is widely used to determine the activation energy for crystallization (E_c) considering the heating rate (β) dependence of the peak crystallization temperature (T_p). The value of E_c can be determined from the slope of a plot of $\ln(T_p^2/\beta)$ vs $1/T_p$ according to the following equation:^{35,42}

$$\ln\left(\frac{T_p^2}{\beta}\right) = \frac{E_c}{RT_p} + \text{constant}, \quad (5)$$

where R is the universal gas constant. A linear plot indicates the validity of the Kissinger method. The value of activation energy for crystallization (E_c) can be calculated using a simplified form of Kissinger equation that, as mentioned before, has been proposed by some authors assuming that the variation of $\ln(1/T_p^2)$ with $\ln \beta$ is much slower than that of $\ln(1/T_p)$ with $\ln \beta$.^{31,41-43}

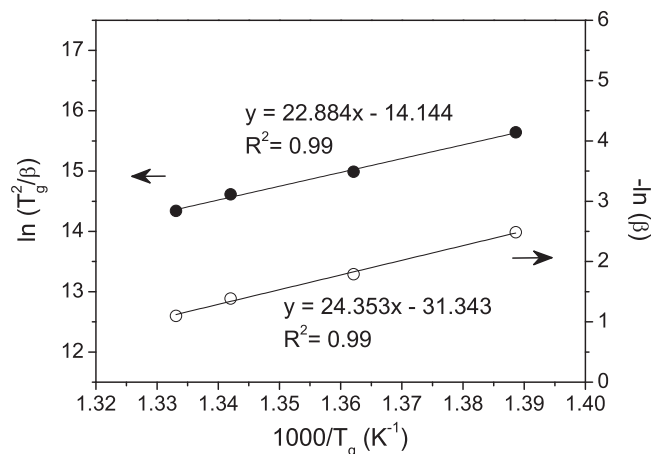


FIG. 5. Plots of $\ln(T_g^2/\beta)$ and of $\ln(\beta)$ vs. $1000/T_g$.

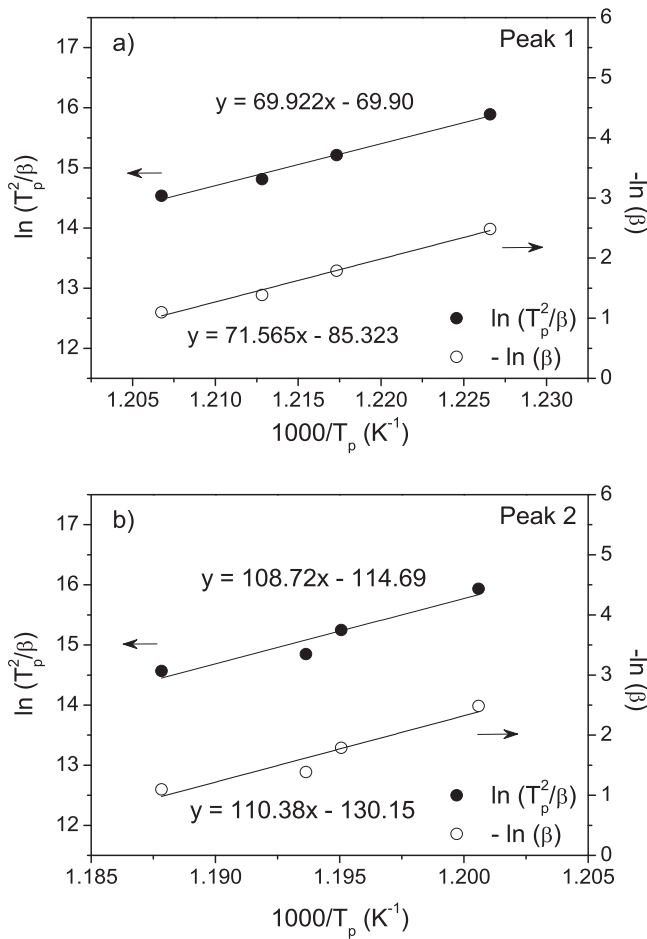


FIG. 6. Plots of $\ln(T_p^2/\beta)$ and of $\ln(\beta)$ vs. $1000/T_p$ for the two exothermic peaks.

$$\ln(\beta) = -\frac{E_c}{RT_p} + \text{constant}. \quad (6)$$

The plot of $\ln(\beta)$ vs $1/T_p$ should be a straight line whose slope also yields the value of E_c . Figure 6 shows the plots of $\ln(T_p^2/\beta)$ and of $\ln\beta$ versus $1000/T_p$. The E_c values determined according to Eqs. (5) and (6) for the first and second exothermic peaks are shown in Table II. The values are close to each other indicating that it is possible to use either of the two approaches.

From Table II, it is observed that E_c increases for the second peak, suggesting that the energy barrier for the glass-crystallization transformation for the second peak is higher than that for the first peak. That is, E_c value for the peak corresponding to the crystallization of barium borate (β -BaB₂O₄) is lower than E_c value for the peak corresponding to the crystallization of barium silicate (Ba₅Si₈O₂₁). These results indicate that the formation of the barium borate

TABLE II. Values of the activation energy for crystallization (E_c) obtained by different equations (kJ/mol).

Equation	First crystallization peak (E_{c1})	Second crystallization peak (E_{c2})
(5)	581	904
(6)	595	918

crystalline phase needs lower activation energy as it is generated in a loose borate-rich glass network structure, while the barium silicate crystalline phase has to be formed in a more interlocked silicate glass network structure.

To study the nature of the crystallization process, the fraction of crystallization (χ) was determined. The area under a DSC crystallization peak, obtained at a constant heating rate, is directly proportional to the volume fraction of crystallites (χ) precipitated in the glass.^{11,22,39,44,45} From the DSC curve, the fraction of crystallization at any temperature T can be determined by the ratio A_T/A , where A is the total area of the crystallization peak between the temperature T_i (where crystallization just begins) and the temperature T_f (where the crystallization is completed) and A_T is the area between T_i and T , as shown schematically in Figure 7. For both exothermic peaks, the variation of the crystallization fraction (χ) as a function of temperature (T) is shown in Figure 8. The curves display a classical sigmoid shape for the different heating rates, indicating that the formation of the crystalline phase proceeds by a combination of nucleation and growth processes.⁴²

The ratio between the ordinates of the DSC curve and the total area of the exothermal peak gives the corresponding crystallization rates,^{11,44} which make it possible to build the curves of the exothermal peaks represented in Figures 9(a) and 9(b). The maxima of the crystallization rate ($d\chi/dt$) values, $(d\chi/dt)_{T_p}$, increase with the increase in the heating rate, which agrees with what has been widely reported in the literature.^{11,42,44}

For both exothermic peaks, taking into account the experimental value of $(d\chi/dt)_{T_p}$ at each heating rate, the value of the Avrami exponent (n) can be calculated from the following equation:^{11,42}

$$n = \frac{(d\chi/dt)_{T_p} \times RT_p^2}{0.37\beta E_c}. \quad (7)$$

For both peaks, the mean value of $\langle n \rangle$ is very close to 2. For the first exothermic peak, corresponding to the crystallization of barium borate (β -BaB₂O₄), the values determined for n are in the range 1.7–2.4, and for the second exothermic

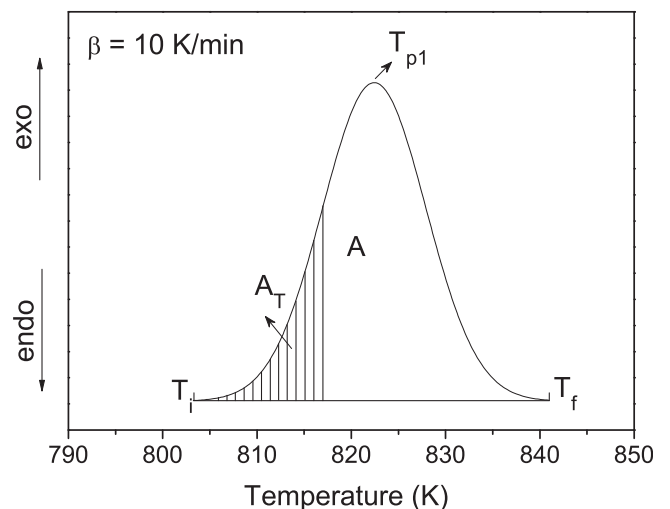


FIG. 7. Area A between T_i and T_f , and area A_T between T_i and T for the first crystallization peak ($\beta = 10$ K/min).

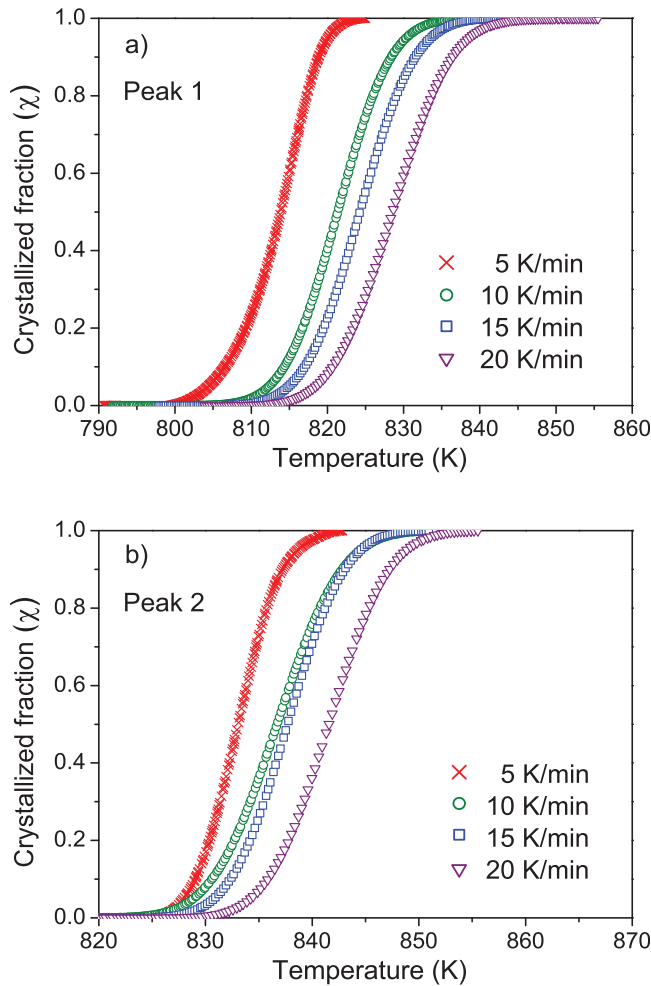


FIG. 8. Crystallized fraction (χ) as a function of temperature at different heating rates for the two overlapped crystallization peaks.

peak, corresponding to the crystallization of barium silicate ($\text{Ba}_5\text{Si}_8\text{O}_{21}$), n values are in the range 1.5–2.1. The value of the kinetic exponent ($n \approx 2$) for this ternary glass ($60\text{BaO}-30\text{B}_2\text{O}_3-10\text{SiO}_2$) is consistent with a crystallization mechanism with one dimensional growth.⁴⁶

In a non-isothermal crystallization process, the volume fraction of crystallites (χ) precipitated at a given temperature (T) in a glass heated at constant rate (β) can be related to the activation energy for crystallization (E_c) and to the Avrami exponent (n) through the following expression suggested by Matusita *et al.*:⁴⁷

$$\ln[-\ln(1 - \chi)] = -n \ln(\beta) - 1.052(n - 1) \left(\frac{E_c}{RT} \right) + \text{const.} \quad (8)$$

From this equation, a plot of $\ln[-\ln(1 - \chi)]$ versus $1000/T$ for each heating rate is expected to be a straight line with a slope of $1.052(n - 1)(E_c/R)$. It is verified that, for the various heating rates, the plots are non-linear over the entire temperature range, as shown in Figure 10. This suggests that there is a variation in E_c and n during the crystallization process of glass.^{48–50}

In fact, some authors have shown that n and E_c values are not necessarily constant but vary during the transformation,

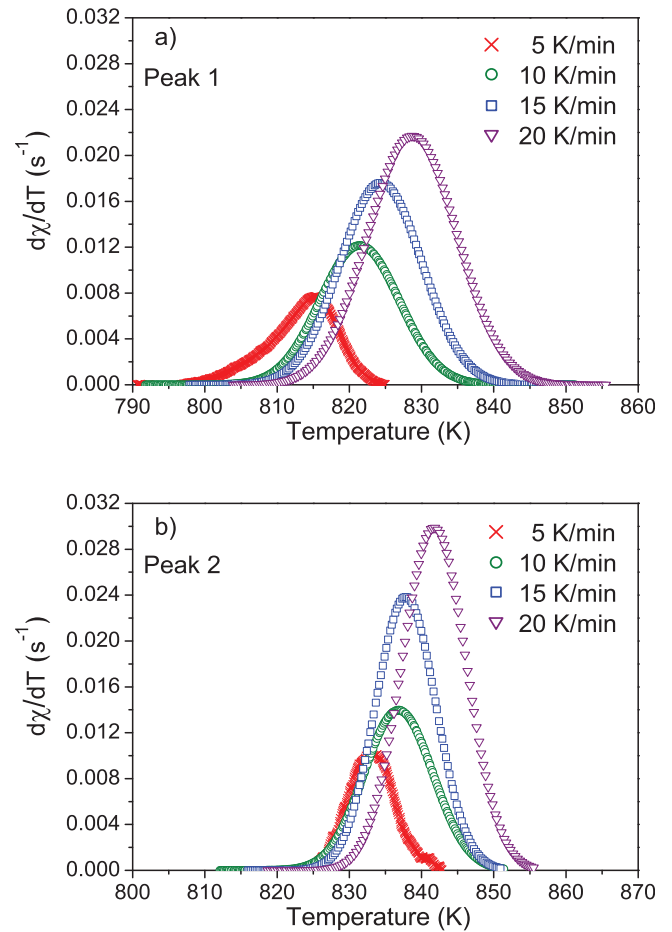


FIG. 9. Crystallization rate as a function of temperature for the first and second exothermal peaks at different heating rates.

both in isothermal⁴⁹ and in non-isothermal methods.^{39,50} The activation energy for different crystallization volume fractions is not constant in the whole transformation due to the change of nucleation and growth behaviors during the crystallization process.⁵⁰ The variation of the activation energy E_c and of the Avrami exponent n can be expressed by the local activation energy $E_c(\chi)$ and the local Avrami exponent $n(\chi)$.^{48,51,52}

The local activation energy $E_c(\chi)$, representing the activation energy for crystallization when the crystallized volume fraction is χ , can be determined from non-isothermal DSC results, using the method proposed by Ozawa, according to the following expression:^{53,54}

$$\left[\frac{d(\ln(\beta))}{d(1/T)} \right]_{\chi} = - \frac{E_c(\chi)}{R}, \quad (9)$$

where R is the gas constant and T and β are the temperature and the heating rate corresponding to the value of χ , respectively. Taking into account the experimental data presented in Figure 8, the plots of $\ln(\beta)$ versus $1000/T$ at various values of χ ($0.1 < \chi < 0.9$) were obtained (Figure 11) and from the slopes the local activation energy, $E_c(\chi)$ values were calculated.

Figure 12 illustrates the change of $E_c(\chi)$ with the crystallized volume fraction (χ) for the two crystallization peaks. It is seen that for the first exothermic peak, corresponding to the

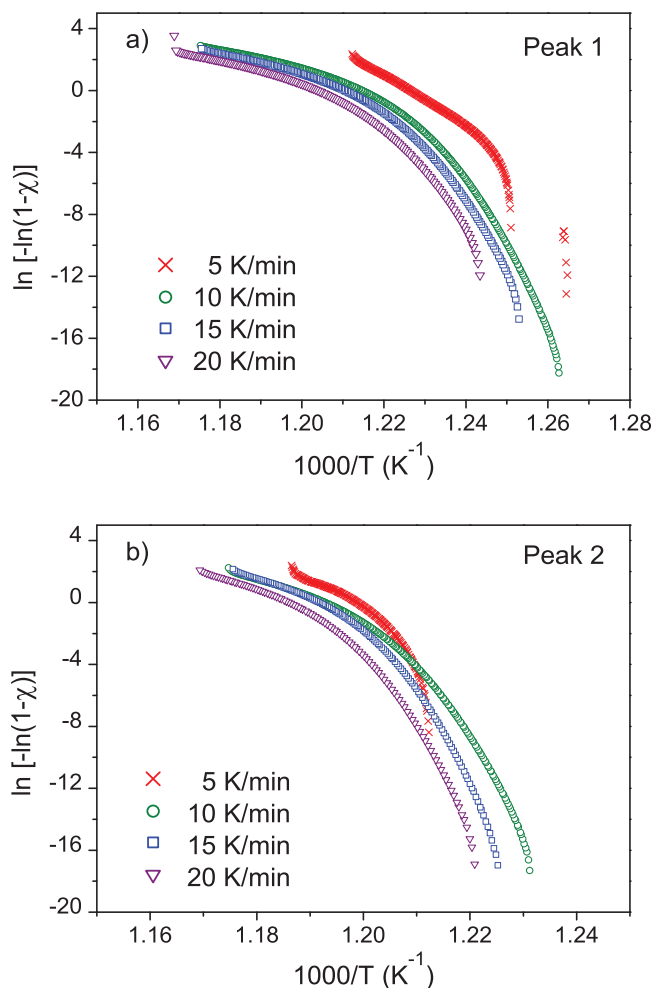


FIG. 10. Plots of $\ln[-\ln(1-\chi)]$ vs $1000/T$ at different heating rates for the two crystallization peaks.

formation of barium borate (β -BaB₂O₄), the local activation energy for crystallization varies slowly along the crystallization process, at the initial stage of the crystallization process ($\chi=0.1$) the value of $E_c(\chi)$ is ~ 554 kJ/mol and then it decreases slowly until ~ 458 kJ/mol for $\chi=0.9$. For the second exothermic peak, associated to the crystallization of barium silicate (Ba₅Si₈O₂₁), the value of $E_c(\chi)$ is higher during the initiation of the crystallization process (~ 1104 kJ/mol) and then it decreases continuously till ~ 831 kJ/mol for $\chi=0.9$. The mean $E_c(\chi)$ values for the first and second exothermic peaks (~ 506 and ~ 968 kJ/mol, respectively) are of the same magnitude as the mean values of E_{c1} and E_{c2} (~ 588 and ~ 911 kJ/mol, respectively) calculated from the values quoted in Table II and obtained by the Kissinger equation, Eq. (5), and simplified Kissinger equation, Eq. (6).

From the prior knowledge of the local activation energy for a non-isothermal crystallization process, $E_c(\chi)$, it is possible to determine the local Avrami exponent, $n(\chi)$, using the following equation:^{39,48}

$$n(\chi) = \frac{-R\partial \ln[-\ln(1-\chi)]}{E_c(\chi)\partial(1/T)}. \quad (10)$$

Taking into account the local activation energy, $E_c(\chi)$, the $n(\chi)$ values at a heating rate of 10 K/min were calculated

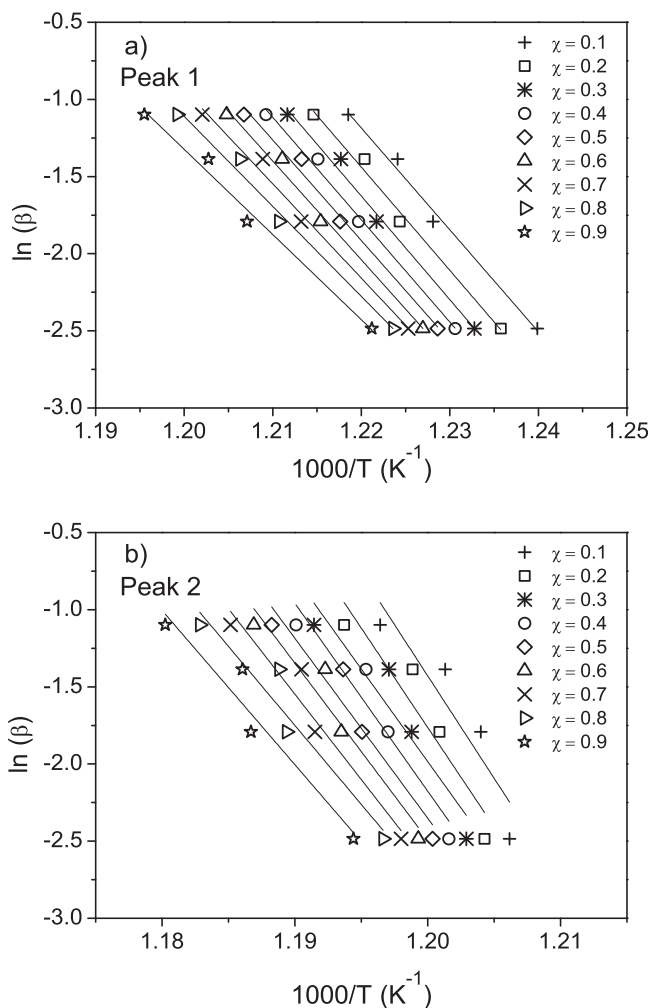


FIG. 11. Plots of $\ln(\beta)$ vs $1000/T$ at various values of χ ($0.1 < \chi < 0.9$) for the two crystallization peaks.

using Eq. (10). The change of the local Avrami exponent, $n(\chi)$, with the fraction of crystallization (χ) for the two exothermic peaks is also presented in Figure 12. For both peaks, the mean value of $n(\chi)$ is very close to 2. This is in

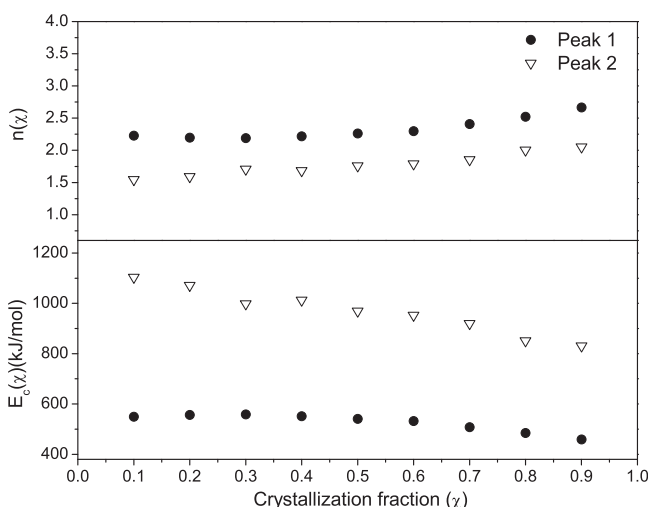


FIG. 12. Local activation energy for crystallization $E_c(\chi)$ and local Avrami exponent $n(\chi)$ as a function of crystallization fraction (χ) at a heating rate of 10 K/min.

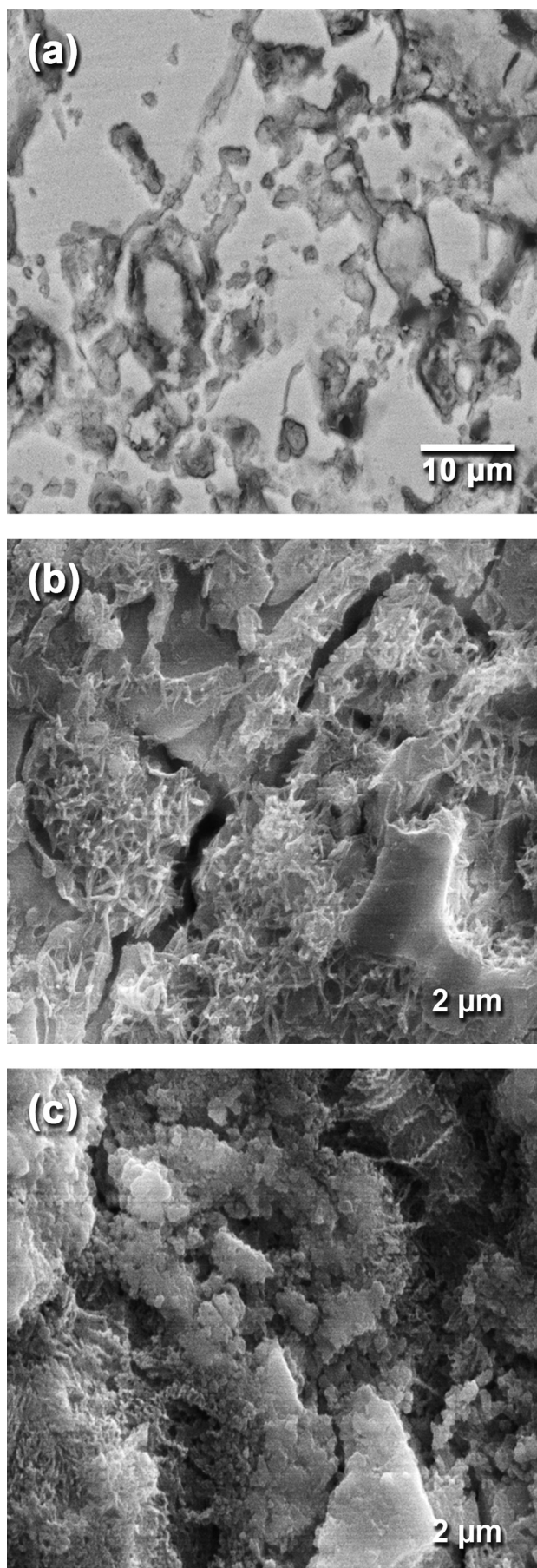


FIG. 13. SEM photographs of glass samples heated at 773 K (a) and (b) and heated at 833 K. Non-etched surface (a); etched surfaces (b) and (c).

agreement with the mean value of $\langle n \rangle$ for both crystallization peaks calculated from Eq. (7), being indicative of a crystallization mechanism with a one-dimensional growth.^{46,55}

To confirm the above statement, the microstructure of thermally annealed samples was examined by a detailed SEM analysis. The micrographs of samples sintered for 1 h at 773 K and at 833 K are depicted in Figure 13. Both micrographs presented in Figures 13(a) and 13(b) correspond to a glass sample that has been heat-treated at 773 K, but with SEM observation carried out in a non-etched and etched polished surface, respectively. The microstructure presented in Figure 13(a) exhibits a large number of zones with a smooth surface, which is a typical feature of glass, and the presence of submicron sized crystallites with acicular shape within the glass is well evidenced after chemical etching of the polished surface, Figure 13(b). The microstructure presented in Figure 13(c), corresponding to a glass sample that has been sintered at a higher temperature (833 K), reveals much less residual glass areas comparatively to that shown in Figure 13(b) with the same magnification, and it shows a fully crystallized material with some crystallites of acicular shape, but most of the crystallites have a more regular morphology.

The uni-dimensional crystallization growth mechanism observed in some glass compositions based on the system $\text{BaO-SiO}_2\text{-B}_2\text{O}_3$, containing additions of other oxides (e.g., MgO , Al_2O_3) has been reported.^{15,16,56} The microstructural observation of such glasses after treatment at higher temperature and longer time than in the present study (1083 K, 1–10 h) revealed barium silicate ($\text{Ba}_5\text{Si}_8\text{O}_{21}$) crystals having a rhombic shape.¹⁵ Also, crystals of elongated shape have been observed in barium-magnesium silicates with B_2O_3 additions used as glass-ceramic sealant compositions for solid oxide fuel cells.^{16,56} The elemental chemical analysis by EDS of the observed crystallites has not been possible because their size is much smaller than the detection width ($\sim 1 \mu\text{m}$) of the microanalysis probe.⁵⁷ Taking into account the above microstructural observations for the heat-treated glass (Figure 13), it is considered that primary crystallization started at the surface of the glass particles with growth of acicular barium borate crystallites and then it was followed by the crystallization of more regular shaped barium silicate crystallites.

IV. CONCLUSIONS

The thermal behavior and crystallization kinetics of a glass with a composition $60\text{BaO-}30\text{B}_2\text{O}_3\text{-}10\text{SiO}_2$ (mol. %) was investigated under non-isothermal conditions by DSC, XRD, and SEM. DSC curves exhibited an endothermic effect near glass transition and two overlapping crystallization exothermic peaks. XRD analysis indicated that the first exothermic peak corresponds to the crystallization of $\beta\text{-BaB}_2\text{O}_4$ phase, whereas the second exothermic peak corresponds to the formation of $\text{Ba}_5\text{Si}_8\text{O}_{21}$ phase. The values of the activation energy for glass transition determined by two different approaches were 190 kJ/mol and 202 kJ/mol. The average activation energy values for the formation of $\beta\text{-BaB}_2\text{O}_4$ and of $\text{Ba}_5\text{Si}_8\text{O}_{21}$ were ~ 588 kJ/mol and ~ 911 kJ/mol, respectively. This indicates that the formation of the barium borate

crystalline phase needs lower activation energy as it is generated in a loose borate-rich glass network structure, while the barium silicate crystalline phase has to be formed in a more interlocked silicate glass network structure.

The values of the local activation energy for crystallization of β -BaB₂O₄ decreased from ~ 554 to ~ 458 kJ mol⁻¹ and for crystallization of Ba₅Si₈O₂₁ decreased from ~ 1104 to ~ 831 kJ mol⁻¹, as the fraction of crystallization varied from 0.1 to 0.9. The Avrami exponent calculated for both exothermic peaks has the same value, $n \approx 2$. SEM observations indicated that surface crystallization with formation of acicular submicron crystallites was the dominant crystallization mechanism at 773 K, but when the sintering temperature of the glass increased to 833 K crystallization progressed from the surface towards the bulk with formation of more regular shape submicron crystallites.

ACKNOWLEDGMENTS

This work was supported by Fundação para a Ciência e a Tecnologia (FCT, Portugal) through Project PTDC/CTM/102141/2008 and through funding to CENIMAT/I3N (Strategic Project PEst-C/CTM/LA0025/2013). Roque Soares is grateful for the PhD Grant (SFRH/BD/87672/2012) from FCT, Portugal.

- ¹E.-S. Lim, B.-S. Kim, J.-H. Lee, and J.-J. Kim, *J. Eur. Ceram. Soc.* **27**, 825 (2007).
- ²E.-S. Lim, B.-S. Kim, J.-H. Lee, and J.-J. Kim, *J. Non-Cryst. Solids* **352**, 821 (2006).
- ³H.-I. Hsiang, C.-S. Hsi, C.-C. Huang, and S.-L. Fu, *Mater. Chem. Phys.* **113**, 658 (2009).
- ⁴S. Chen, S. Zhang, X. Zhou, T. Zhang, and M. He, *J. Alloys Compd.* **498**, 185 (2010).
- ⁵N. Santha, S. Shamsudeen, N. T. Karunakaran, and J. I. Naseemabeevi, *Int. J. Appl. Ceram. Technol.* **8**, 1042 (2011).
- ⁶S. Chen and D. Zhu, *J. Alloys Compd.* **536**, 73 (2012).
- ⁷Z. Wang, Y. Hu, H. Lu, and F. Yu, *J. Non-Cryst. Solids* **354**, 1128 (2008).
- ⁸R. C. C. Monteiro, A. A. S. Lopes, M. M. A. Lima, J. P. Veiga, R. J. C. Silva, C. J. Dias, E. J. R. Davim, and M. H. V. Fernandes, *J. Am. Ceram. Soc.* **95**, 3144 (2012).
- ⁹G.-H. Hwang, H.-J. Jeon, and Y.-S. Kim, *J. Am. Ceram. Soc.* **85**, 2956 (2002).
- ¹⁰E.-S. Lim, B.-S. Kim, J.-H. Lee, and J.-J. Kim, *J. Electroceram.* **17**, 359 (2006).
- ¹¹A. Arora, E. R. Shaaban, K. Singh, and O. P. Pandey, *J. Non-Cryst. Solids* **354**, 3944 (2008).
- ¹²J.-H. Jean, Y.-C. Fang, S. X. Dai, and D. L. Wilcox, *J. Am. Ceram. Soc.* **84**, 1354 (2001).
- ¹³J. Ramkumar, S. Chandramouleeswaran, V. Sudarsan, R. K. Mishr, C. P. Kaushik, K. Raj, and A. K. Tyagi, *J. Hazard. Mater.* **172**, 457 (2009).
- ¹⁴A. Goel, D. U. Tulyaganov, I. K. Goel, E. R. Shaaban, and J. M. F. Ferreira, *J. Non-Cryst. Solids* **355**, 193 (2009).
- ¹⁵D. Godeke and U. Dahlmann, *J. Power Sources* **196**, 9046 (2011).

- ¹⁶M. J. Pascual, C. Lara, and A. Duran, *Phys. Chem. Glasses: Eur. J. Glass Sci. Technol., Part B* **47**, 572 (2006).
- ¹⁷L. Rezazadeh, S. Baghshahi, A. N. Golikand, and Z. Hamnabard, *Ionics* **20**, 55 (2014).
- ¹⁸V. Kumar, O. P. Pandey, and K. Singh, *Physica B* **405**, 204 (2010).
- ¹⁹V. V. Golubkov, V. L. Stolyarova, Z. G. Tyumina, and N. G. Tyumina, *Glass Phys. Chem.* **36**, 554 (2010).
- ²⁰T. Mullenbach, M. Franke, A. Ramm, A. R. Betzen, S. Kapoor, N. Lower, T. Munhollon, M. Berman, M. Affatigato, and S. A. Feller, *Phys. Chem. Glasses: Eur. J. Glass Sci. Technol., Part B* **50**, 89 (2009).
- ²¹M. Erol, S. Küçükbayrak, and A. E-Meriçboyu, *J. Non-Cryst. Solids* **355**, 569 (2009).
- ²²M. Ghasemzadeh, A. Nemati, A. Nozad Golikand, Z. Hamnabard, and S. Baghshahi, *Synth. React. Inorg. Met.-Org., and Nano-Met. Chem.* **41**, 561 (2011).
- ²³B. Shanmugavelu and V. V. R. K. Kumar, *J. Am. Ceram. Soc.* **95**, 2891 (2012).
- ²⁴J. Vázquez, P. L. López-Alemány, P. Villares, and R. Jiménez-Garay, *J. Phys. Chem. Solids* **61**, 493 (2000).
- ²⁵H. E. Kissinger, *J. Res. Natl. Bur. Stand.* **57**, 217 (1956).
- ²⁶C. T. Moynihan, A. J. Easteal, J. Wilder, and J. Tucker, *J. Phys. Chem.* **78**, 2673 (1974).
- ²⁷W. A. Johnson and R. F. Mehl, *Trans AIME* **135**, 416 (1939).
- ²⁸M. Avrami, *J. Chem. Phys.* **7**, 1103 (1939).
- ²⁹M. Avrami, *J. Chem. Phys.* **8**, 212 (1940).
- ³⁰M. Avrami, *J. Chem. Phys.* **9**, 177 (1941).
- ³¹H. Yinnon and D. R. Uhlmann, *J. Non-Cryst. Solids* **54**, 253 (1983).
- ³²H. E. Kissinger, *Anal. Chem.* **29**, 1702 (1957).
- ³³A. B. Selçuk and H. Yavuz, *Mater. Lett.* **57**, 4382 (2003).
- ³⁴D. W. Henderson, *J. Therm. Anal.* **15**, 325 (1979).
- ³⁵K. Matusita and S. Sakka, *J. Non-Cryst. Solids* **38–39**, 741 (1980).
- ³⁶S. Z. Xiao, *J. Non-Cryst. Solids* **45**, 29 (1981).
- ³⁷M. Lasocka, *Mater. Sci. Eng.* **23**, 173 (1976).
- ³⁸O. S. Narayanaswamy, *J. Am. Ceram. Soc.* **54**, 491 (1971).
- ³⁹K. Majhi and K. Varma, *J. Mater. Sci.* **44**, 385 (2009).
- ⁴⁰A. Abu-Sehly, *Mater. Chem. Phys.* **125**, 672 (2011).
- ⁴¹S. Mahadevan, A. Giridhar, and A. K. Singh, *J. Non-Cryst. Solids* **88**, 11 (1986).
- ⁴²J. Vázquez, C. Wagner, P. Villares, and R. Jiménez-Garay, *J. Non-Cryst. Solids* **235**, 548 (1998).
- ⁴³T. Ozawa, *Polymer* **12**, 150 (1971).
- ⁴⁴K. A. Aly, A. A. Othman, and A. M. Abousehly, *J. Alloys Compd.* **467**, 417 (2009).
- ⁴⁵C.-R. Chang and J.-H. Jean, *J. Am. Ceram. Soc.* **82**, 1725 (1999).
- ⁴⁶R. Iordanova, E. Lefterova, I. Uzunov, and D. Klissurshi, *J. Therm. Anal. Calorim.* **70**, 393 (2002).
- ⁴⁷K. Matusita, T. Komatsu, and R. Yokota, *J. Mater. Sci.* **19**, 291 (1984).
- ⁴⁸W. Lu, B. Yan, and W. Huang, *J. Non-Cryst. Solids* **351**, 3320 (2005).
- ⁴⁹A. A. Abu-Sehly, S. N. Alamri, and A. A. Joraid, *J. Alloys Compd.* **476**, 348 (2009).
- ⁵⁰A. A. Joraid, S. N. Alamri, and A. A. Abu-Sehly, *J. Non-Cryst. Solids* **354**, 3380 (2008).
- ⁵¹A. Calka and A. P. Radlinski, *Mater. Sci. Eng.* **97**, 241 (1988).
- ⁵²K. Lu and J. T. Wang, *Mater. Sci. Eng., A* **133**, 500 (1991).
- ⁵³T. Ozawa, *J. Therm. Anal.* **2**, 301 (1970).
- ⁵⁴T. Ozawa, *J. Therm. Anal.* **31**, 547 (1986).
- ⁵⁵T. Sun, H. Xiao, Y. Cheng, and H. Liu, *Ceram. Int.* **35**, 1051 (2009).
- ⁵⁶M. J. Pascual, A. Guillet, and A. Duran, *J. Power Sources* **169**, 40 (2007).
- ⁵⁷J. I. Golstein, D. E. Newbury, P. Echlin, D. C. Joy, A. D. Romig, Jr., C. E. Lyman, C. Fiori, and E. Lifshin, "Scanning electron microscopy and x-ray microanalysis," in *A Text for Biologists, Materials Scientists, and Geologists* (Plenum Press, New York, 1992), p. 417.